Analyst

Accepted Manuscript

This is an *Accepted Manuscript*, which has been through the Royal Society of Chemistry peer review process and has been accepted for publication.

Accepted Manuscripts are published online shortly after acceptance, before technical editing, formatting and proof reading. Using this free service, authors can make their results available to the community, in citable form, before we publish the edited article. We will replace this *Accepted Manuscript* with the edited and formatted *Advance Article* as soon as it is available.

You can find more information about *Accepted Manuscripts* in the Information for Authors.

Please note that technical editing may introduce minor changes to the text and/or graphics, which may alter content. The journal's standard Terms & Conditions and the Ethical guidelines still apply. In no event shall the Royal Society of Chemistry be held responsible for any errors or omissions in this *Accepted Manuscript* or any consequences arising from the use of any information it contains.

ROYAL SOCIETY OF CHEMISTRY

www.rsc.org/analyst

Journal Name RSCPublishing

ARTICLE

Label-free determination of lipids composition and secondary proteins structure of human salivary noncancerous and cancerous tissues by Raman microspectroscopy

Cite this: DOI: 10.1039/x0xx00000x

Received 00th January 2012,
Accepted 00th January 2012

DOI: 10.1039/x0xx00000x

www.rsc.org/

Beata Brozek-Pluska,[a*] Monika Kopec,[a] Izabela Niedzwiecka[b] and Alina Morawiec-Sztandera[b]

The applications of optical spectroscopic methods in cancer detection open new possibilities in oncological diagnostics. Raman spectroscopy and Raman imaging represent noninvasive, label-free, and rapidly developing tools in cancer diagnosis. In the study described in this paper Raman microspectroscopy has been employed to examine noncancerous and cancerous human salivary glands tissues of the same patient. The most significant differences between noncancerous and cancerous tissues were found in regions typical for the vibrations of lipids and proteins. The detailed analysis of secondary structure of proteins contained in the cancerous and the noncancerous tissues is also presented.

Introduction

The human salivary glands are divided into major and minor salivary gland categories. The major salivary glands are the parotid, the submandibular, and the sublingual glands. The minor glands are dispersed throughout the upper aerodigestive submucosal ie, palate, lip, pharynx, nasopharynx and larynx, piriform recess.

The anatomy of salivary glands was described the first time by Beahrs and Adson in the 60's of the XX-th century. They described also firstly surgical landmarks for avoiding injury to the main trunk and branches of the facial nerve and advocated complete removal of the superficial portion of the parotid gland for noninvasive lesions.[1]

Salivary gland cancers comprise about 3-6 % of all head and neck human cancers and cause < 0.1 % of all cancer deaths.[2] Most of them are detected in the sixth or seventh decade of life with the same frequency in both sexes. In 70-80 % the parotid gland tumors are benign, in the submandibular more than a half are malignant.[3]

The great variety of histological types of salivary glands makes them a major challenge for radiologists and clinicians, simultaneously the large range of differential diagnoses significantly influences the prognosis and the treatment; the choice of the appropriate treatment method determines the probability of a survival for the patient.

Pleomorphic adenomas (benign mixed tumors) are the most common tumors of the salivary gland and are most often located in the tail of the parotid gland. When they are located in the minor salivary glands most often can be found in the hard palate. Microscopically, benign mixed tumors are characterized by variable, diverse, structural histologic patterns. They can form structures of sheets, strands, or islands of spindle and stellate cells, with a myxoid configuration occasionally predominating. Treatment of benign neoplasms involves the complete surgical excision of the affected gland.

Only a few clinical symptoms, such as facial nerve palsy, in patients with parotid gland masses allow the diagnosis of malignancy. In most cases of palpable tumours the differentiation between benign and malignant types is possible only by a clinical examination.[3,4] For malignant changes the most popular type is a squamous cell carcinoma.

In the traditional clinical approach cancer is identified by histopathological analysis or by different well established imaging methods, such as computer tomography (CT), magnetic resonance imaging (MRI), positron emission tomography (PET), X-ray, ultrasound. The histological analysis, is the standard procedure of cancer identification. Spectroscopic methods open up new possibilities of diagnostics, they are noninvasive, allow the diagnosis in a short time and what is most important provide chemical information of normal, benign and malignant types of tissues.

A special place among new, fast developing spectroscopic methods belongs to Raman spectroscopy (RS) and Raman imaging (RI). In last few years it has been proved that RS and RI are especially useful for breast cancer detection and differentiation.[5-18] However, RS and RI can cover a broad spectrum of diagnostic applications, including for example: skin diseases, body fluids analysis, Alzheimer's disease.[19-22] The hudge advantage of RS and RI is that the current instrumentation of Raman techniques has enabled a fast analysis of different cancer and normal tissues samples including histological sections, bulk tissues and single living cells.[23-25] The superiority of RS and RI over other methods

Analyst Accepted Manuscript

results also from fact that they can monitor the tissue without any external agents so they can analyze pure, unaltered tissue mimicking tissue in the human body. Moreover, novel solutions such TERS technique (TERS - Tip Enhanced Raman Spectroscopy) provide very high spatial resolution enabling the observation of the detailed cell anatomy. The TERS technique was succesfully used in RNA sequensing.[26]

Because RS in cancer diagnostic allows to receive a detailed information about chemical composition (lipids, proteins, carbohydrates, water content) of the examinated tissue and to avoid ambiguous prone to human interpretations this technique can give valuable contribution especially in determining of the safety margin, which is normally removed during a surgery. Chemical changes in tissues can occur before the physical changes are observed, so optical methods can monitor cancer changes in an earlier stage than histopatological analysis, it is especially important for surgery in a head and neck regions, where the safety margin should be minimal; the extensive surgery can impaired the important life functions and may result facial deformities.

To the best of our knowledge, the analysis of the lipids profile and the secondary structure of proteins of the cancerous and the noncancerous tissues of salivary glands of the same patient have not been previously reported.

Experimental

Patients and samples

In the described study, Raman spectroscopy and Raman imaging have been employed to analyze human salivary cancer specimens. All procedures were conducted under a protocol approved by the Bioethical Committee at the Medical University of Lodz (RNN/45/14/KE/11/03/2014). Total number of patients was 20. Total number of samples was 49. For each patient the two types of tissues: the tissue form the safety margin and the tissue from the tumor mass were analysed. Thousands of spectra for biological samples were recorded using Raman Imaging and Raman spectroscopy. All tissue samples were snap frozen and stored at -80 ºC. One part of each type was cryosectioned with a microtome (Microm HM 550, Sermed) into 6 μm-thick sections for Raman analysis. The thin cryosectioned tissue samples (without staining and paraffin embedding) have been examined by Raman imaging. After Raman analysis these sections were stained and histologically examined. The adjacent part of the tissue was paraffin embedded and also cut into 6 μm-thick sections for typical histological analysis. More detail about the tissue preparation can be found elsewhere.[7,27]

Instrumentation

Raman microspectroscopy and imaging

Raman spectra and images were obtained with alpha 300 RSA (WITec, Ulm, Germany) model equipped with an Olympus microscope coupled via the fiber of 50 μm core diameter with an monochromator Acton SP 2300i and a CCD Camera Andor Newton DU970N-UVB-353 operating in standard mode with 1600x200 pixels, at -60°C with full vertical binning. The incident laser beam (doubled SHG of the Nd:YAG laser (532 nm)) of alpha 300 RSA was focused on the sample through a 40x dry objective (Nikon, objective type CFI Plan Fluor C ELWD DIC-M, numerical aperture (NA) of 0.60, and a 3.6-2.8 mm working distance) to the spot of 650 nm. The average laser excitation power was 10 mW, with an integration time of 0.3 sec. Rayleigh scattered light was removed using an edge filter. A piezoelectric table was used to record Raman images. Spectra were collected at one acquisition per each pixel and a 1200 lines/mm diffraction grating. Prior to the basis analysis, each spectrum was processed to remove cosmic rays, increase the signal-to-noise ratio via spectral smoothing (Savitzky-Golay method) subtract a baseline arising from the (CaF_2) substrate and biological autofluorescence. The large number of spectra collected in this study required the use of automated removal method for all the spectra, which is critical to remove sources of variability arising from autofluorescence and substrate contamination. After baseline removal, the dominant remaining source of distinction between spectra is the intensity of the Raman features, arising from the variable amount of biological material within the sample. Data acquisition and processing was performed using WITec Project 2.10.

Data analysis method

2D arrays of thousands of individual Raman spectra were evaluated by the basis analysis. In the basis analysis method each measured spectrum of the 2D spectral array is compared to the basis spectra using a least square fit. The basis spectra are created by averaging over various areas of the scanned surface or by using the cluster analysis. The weight factor in each point is represented as a 2D image of the corresponding color and mixed coloring component. It tries to minimize the fitting error D described by the equation (1)

$$D = \left(\overrightarrow{[RecordedSpectrum]} - a \times \overrightarrow{BS_A} - b \times \overrightarrow{BS_B} - c \times \overrightarrow{BS_C} - \cdots\right)^2 \quad (1)$$

by varying the weighting factors *a, b, c, ...* of the basis spectra $\overrightarrow{BS}$.[28]

Results and discussion

In this section, the results of the Raman studies on the noncancerous and the cancerous human salivary gland tissues of the same patient P13 are presented.

The typical Raman spectra and Raman imagings of the noncancerous and the cancerous salivary gland tissues are presented in Figures 1 and 2.

Figure 1

Fig. 1 Microscopy, Raman images and Raman spectra of the noncancerous salivary tissue of the patient P13. (A) Microscopy image (500x500 μm) composed of several single video images of the noncancerous salivary tissue, (B) Raman image (400x200 μm, resolution 1 μm) of the cryosectioned salivary tissue from the region marked in (A) obtained by the basis analysis, (C) images for the filters for spectral regions: 1230-1260 cm^{-1}, 1650-1680 cm^{-1}, 2850-2950 cm^{-1}, 2900-3010 cm^{-1} (D) Raman spectra of the noncancerous salivary tissue. The colours of the Raman spectra in (D) correspond to the colours in the Raman image (B). Mixed areas are displayed as mixed colours. Integration time: 0.3 sec.

Figure2

Fig. 2 Microscopy, Raman images and Raman spectra of the cancerous salivary tissue of the patient P13. (A) Microscopy image (500x500 μm) composed of several single video images of the cancerous salivary tissue, (B) Raman image (350x350 μm, resolution 1 μm) of the cryosectioned salivary tissue from the region marked in (A) obtained by the basis analysis, (C) images for the filters for spectral regions: 1230-1260 cm^{-1}, 1650-1680 cm^{-1}, 2850-2950 cm^{-1}, 2900-3010 cm^{-1} (D) Raman spectra of the cancerous salivary tissue. The colours of the Raman spectra in (D) correspond to the colours in the Raman image (B). Mixed areas are displayed as mixed colours. Integration time: 0.3 sec.

Analyst Accepted Manuscript

This journal is © The Royal Society of Chemistry 2012

One can see from Figures 1 and 2 that using Raman spectroscopy the inhomogeneous distribution of different tissue components can be monitored. The spectral region 400-1800 cm^{-1} is characteristic for vibrations of DNA/RNA, lipids and proteins, the region 2600-3200 cm^{-1} is typical for lipids, proteins, and water vibrations.

To monitor the accumulation and spatial distribution of the individual components in the noncancerous and the cancerous salivary gland tissues: lipids, fatty acids, and proteins Raman filters presented in Figure 1C and 2C were used. The spectral regions 1230-1260 cm^{-1} and 1650-1665 cm^{-1} correspond to Amide III and Amide I vibrations respectively, the spectral range 2850-2950 cm^{-1} is typical for fatty acids and triglycerides, when the range 2900-3010 cm^{-1} is typical for vibrations of proteins.

The results presented in Figure 1C and 2C clearly indicate that Raman imaging is a suitable technique to monitor qualitatively and quantitatively the composition of tissues. Comparison of results for different filters shows that in regions rich in lipids and fatty acids a lower concentration of proteins is observed. This observation is consistent with those obtained for the breast tissue samples in our previous studies, where the contribution from the monounsaturated fatty acids and their derivatives, common constituents of triglycerides of the adipose tissue, dominates the Raman spectrum of the noncancerous tissue in contrast with the Raman spectra of the cancerous tissue dominated by proteins.[5,7-9]

Figure 3 demonstrates the comparison of the mean Raman spectra of the noncancerous and the cancerous salivary gland tissues of the same patient P13 into spectroscopic regions: 400-1800 cm^{-1} and 2600-3200 cm^{-1}.

Figure 3

Fig. 3 Comparison of the mean Raman spectra of the noncancerous and the cancerous salivary tissues of the same patient P13, into spectroscopic regions (A) 400-1800 cm^{-1} and (B) 2600-3200 cm^{-1}.

One can see in Figure 3 that spectra of the noncancerous and the cancerous tissues represent peaks typical for lipids, proteins and water.

The Raman spectrum of the noncancerous tissue of the salivary gland in the spectral region 400 – 800 cm^{-1} is dominated by vibrations at ca.: 767, 1080, 1257, 1304, 1332, 1444, 1660 and 1750 cm^{-1} while the spectrum for the cancerous tissue of the salivary gland is dominated by peaks at ca. 756, 785, 830, 860, 930, 1004, 1080, 1135, 1248, 1290, 1343, 1454 and 1670 cm^{-1}. These peaks can be attributing to the vibration typical for DNA/RNA, lipids, phospholipids and proteins.

The main differences in the spectral region 2600-3200 cm^{-1} for the noncancerous and the cancerous salivary tissues are observed for frequencies at 2854, 2888, 2917, 2940 and 3009 cm^{-1} (Figure 3B). For the noncancerous salivary gland tissue all peaks observed at 2854, 2888, 2917, 2940 cm^{-1} are intense, while the spectrum for the cancerous tissue is dominated only by two vibrations at 2917 and 2940 cm^{-1}. Vibrations at 2854, 2888, and 3009 cm^{-1} are typical for lipids and unsaturated lipids, while the vibrations at 2917 and 2940 cm^{-1} can be describes as a combination of the vibrations of lipids and proteins.

The observed wavenumbers of Raman spectra and their tentative assignments are presented in Table 1.

Table 1. Characteristic Raman peaks for the noncancerous and the cancerous salivary gland tissues and their tentative assignments [7,10,29]

Wavenumber / cm^{-1}		Tentative assignments
Noncancerous tissue	Cancerous tissue	
767	756	Nucleic acid, DNA/RNA, phospholipid (choline)
	785	Nucleic acid, DNA/RNA
	830	Nucleic acids, DNA/RNA, Proteins (O-P-O) antisym. str./ring br. Tyrosine
	930	Hydroxyproline/Collagen backbone (C-C)
	1004	Phenylalanine ring br. of proteins
1080	1080	Phpspholipids, O-P-O sym. str.
	1135	Collagen (C-C)
	1248, 1290	Nucleic Acids (T, A), DNA/RNA/Proteins (Amide III)/Lipid, phospholipid (=C-H
1304		Lipids, phospholipids ($C-H_2$) tw.
1332	1343	DNA/RNA, Proteins CH bend.
1444	1454	Fatty acids, triglicerides, CH_2, CH_3 deformation/lipids/proteins C-H wag.
1660		Proteins Amide I/ Unsaturated fatty acids α helix, (C=O) str., (C-H) def./(C=C) str.
	1670	Amide I, β-sheet
1750		C=O
2854		Fatty acids, triglicerides ($C-H_2$) sym. str.
2888		Lipids ($C-H_2$) antisym. str.
	2917	Lipids (CH_3) str.
	2940	Lipids/Proteins (CH_3) antisym. str.
3009		Lipids (=C-H) str.
	3311	Interfacial water

Abbreviations: (bend.) bending, (wag.) wagging, (tw.) twist, (sym.) symmetric, (antisym.) antisymmetric, and (str.) stretch

Analyzing maximum peak positions for vibrations of lipids and proteins in Figure 3 and Table 1 the non-negligible differences for the noncancerous and the cancerous human salivary tissues can be observed. Moreover all peaks corresponding to proteins are more intense in the cancerous tissue compared to the noncancerous one. This finding corresponds to the fact that in contrast to normal cells, the abnormal cells divide in uncontrolled process of the cell growth and synthesize large amounts of proteins. This observation confirms also that the metabolism of these two types of tissues is significantly different. From Figure 3 one can conclude also that the Raman spectrum typical for the cancer tissue reveal intense peaks for DNA and RNA vibrations, what correlates with a high mitotic index of these type of cells. Figure 3 confirms that the main role in a differentiation of the noncancerous and the cancerous

Analyst Accepted Manuscript

tissue is played by lipids especially in a spectral range 2600-3200 cm^{-1} too.

The most characteristic bands observed by Raman spectroscopy for proteins are Amide bands: Amide A (NH stretching about 3500 cm^{-1}), Amide B (NH stretching about 3100 cm^{-1}), and Amide I to VII; I: 1600-1690 cm^{-1} stretching vibration of C=O, II: 1480- 1580 cm^{-1} C-N stretching and N-H bending, III: 1230-1300 cm^{-1} C-N stretching and N-H bending, IV: 625-770 cm^{-1} OCN bending, V: 640-800 cm^{-1} NH bending, VI: 540-600 cm^{-1} out of plane C=O bending, VII: 200 cm^{-1} skeletal mode.

All mentioned above proteins vibrations can be used to characterize two most important types of the secondary structure of proteins: α-helix and β-sheet. The secondary structure of proteins describes certain repetitive, local conformations that are found in most peptide chains and does not describe the actual folding the protein in three dimensions, but instead illustrates the structure of small regions of the peptide. In α-helix structure every backbone N-H group donates a hydrogen bond to the backbone C=O group of the amino acid four residues earlier. The most detailed experimental evidence for α-helix structure comes from atomic-resolution X-ray crystallography.[30] The formation of the α-helix determines ability to create the maximum number of hydrogen bonds, assisted with van der Waals interactions occurring in the core of a densely packed structure. The ideal α-helix structure can be compromised due to the presence of some amino acids such as glycine for example, due to small size of such a peptide molecule. Predominating multiple helices have a hydrophobic group on one side of the helix and the hydrophilic groups on the other side. This property allows α-helixes creating bridges between polar and non-polar regions. Thanks to these properties, grouped helixes can create specific channels enabling the hydrophobic molecules to pass through cell membranes.[31] The β-structure is a second well known structure of proteins. In β-structure amino acid residues viewed along the edges form a harmonica, or pleated sheet. The majority of β strands are arranged adjacent to other strands and form an extensive hydrogen bond network with their neighbors in which the N-H groups in the backbone of one strand establish hydrogen bonds with the C=O groups in the backbone of the adjacent strands. There are two types of β-sheet structure: parallel und unparallel.[31]

The secondary structure of proteins using Raman spectroscopy was studied by Lippert et all.[32] Lippert and co-workers developed the first quantitative analysis method of secondary structure of proteins based on Amide I and Amide III maximum peak positions but the method was limited to the proteins dissolved in water. Williams and Dunker developed the first method based on reference spectra. In the study they focused on Amide I vibration.[33] Berjot et al. computed the reference spectra of different 17 proteins with known secondary structure.[34] Some recent presented studies by Rygula et al. also confirm a correlation between the position of Amide vibrations with the secondary structure of proteins: α-helix, β-sheet, α/β and α+β structure for commercially available proteins.[35]

It has been shown in literature that for α-helix proteins the most specific Amide band observed in Raman spectra is a band at ca. 1345 cm^{-1} assigned to C-Cα-H bending and C-Cα stretching as well as the band at ca. 740 cm^{-1}, which is attributed to Amide IV: the carbonyl in-plane bending vibration.[35,36]

The Amide I mode for α-helix appears for the same regions for Raman and IR spectra at ca. 1650-1660 cm^{-1}. For the β-sheet conformation mode the Amide I vibrations is very strong in Raman spectrum ca. 1670 cm^{-1}. The Amide I band for disordered form of proteins is found ca. 1665 cm^{-1} in Raman spectra.[28,33,34]

Amide III vibrations also shows differences in peaks positions for ordered and disordered forms of proteins. For β-sheet form Amide III vibrations can be observed ca. 1230-1240 cm^{-1} while for disordered forms peaks are observed ca. 1245 cm^{-1}, α-helix conformation doesn't show any strong peaks in this spectral region.[28,33,34]

We will show that all differences observed for maximum peak positions for Amide vibrations for salivary gland tissues correlate also with lesions, cancer changes in human body and a secondary structure of proteins.[28]

One can see from Figure 3 that for the noncancerous tissue peaks at ca. 767 and 1332 cm^{-1} are observed. These two peaks confirm clearly the α-helix structure of proteins. We cannot observe also any peaks in the spectral range 1235-1240 cm^{-1} for this type of tissue. This fact confirms the lack of β-sheet structure of proteins in the noncancerous human salivary tissue. The α-helix structure of proteins in this type of tissue is also confirmed by the Amide I region where the vibration at ca. 1660 cm^{-1} is observed. For the cancerous tissue one can find peaks at ca. 1670 cm^{-1} in Amide I region which suggested the β-sheet structure of proteins. In the Amide III region the broad peak ranging from 1235 to 1260 cm^{-1} with the maximum at ca. 1248 cm^{-1} also confirms the presence of β-form but some disordered structure of proteins in this spectral range also should be taken into account. The vibrations at 1267 cm-1 for the noncancerous tissue confirms not negligible contribution of disordered forms fundamentally. The differentiation of β-structure and disordered forms of proteins is unfortunately very difficult. The intense peaks at ca. 830/860 cm^{-1} can be attributed to tyrosine doublet. For the cancer tissue peaks typical for collagen at 930 and 1135 cm^{-1} are also observed.

Form Figure 3B many differences between the noncancerous and the cancerous tissues in a spectral region of 2600-3200 cm^{-1} can be found also. In the noncancerous tissue the Raman spectrum is dominated by peaks at ca. 2854, 2888, 2917 and 3009 cm^{-1}. The vibrations centered at 2854, 2888, and 3009 cm^{-1} are typical for lipids and unsaturated fatty acids. The most important difference between the noncancerous and the cancerous tissues can be observed for 2917 and 3009 cm^{-1}. The peak at ca. 2917 cm^{-1} is typical for CH vibrations in lipids and proteins. The lack of the vibration 3009 cm^{-1} in the cancerous tissue can be attributed to the absence of unsaturated lipids and unsaturated fatty acids typical for the noncancerous type of tissues.[7]

Summarizing the detailed inspection in Figure 3 shows that the α-helix structure of proteins and features of unsaturated fatty acids and unsaturated lipids are typical for the noncancerous human salivary gland tissue while many peaks characteristic for the β-sheet structure and saturated lipids can be observed for the cancerous tissue of the salivary glands.

These findings are in agreement with observations whose confirm that β-sheet structure or the lack of the α-form of proteins are typical for various disease states such as: the contagious spongiform encephalopathies related to the functioning of the PrP – the Prion related Proteins, Alzheimer disease related to presence of β-amyloid or β-thalassemia related to the lack of α-hemoglobine stabilizing protein.[31,37,38]

Analyst Accepted Manuscript

This journal is © The Royal Society of Chemistry 2012

Conclusions

Experimental results presented in this paper proved that Raman spectroscopy and imaging are suitable to characterize the human salivary noncancerous and cancerous tissues.
RI provides information about the spatial distribution of the noncancerous and the cancerous cells and can supply precise information about the boundary of the cancer mass.
Presented results show also that optical methods can help in objective diagnosis independent on pathologist experience based on vibrations typical for proteins and lipids.
RS and RI can be successfully use to determine the secondary structure of proteins based on Amide vibrations. Vibrations typical for α-helix and β-sheet structures can be easily identified in Raman spectra.
Lipids and proteins vibrations can be treated as Raman biomarkers of cancerogenesis.
RS analysis is fast and none special tissue samples preparation is needed.

Acknowledgements
The project was funded through a Dz. St 2014.

Notes and references

[a] Lodz University of Technology, Institute of Applied Radiation Chemistry, Laboratory of Laser Molecular Spectroscopy, Wroblewskiego 15, 93-590 Lodz, Poland.
[b] Medical University of Lodz, Department of Head and Neck Cancer, Kosciuszki 4, 90-419 Lodz, Poland.
*To whom correspondence should be addressed: Beata Brozek-Pluska, Lodz University of Technology, Institute of Applied Radiation Chemistry, Laboratory of Laser Molecular Spectroscopy, Wroblewskiego 15, 93-590 Lodz, Poland, telephone number: +48 42 6313188, fax: +48 42 684-00-43, e-mail: brozek@mitr.p.lodz.pl.

1. O. H. Behrs and M. A. Adson, *Am. J. Surg. Jun*., 1958, **95**, 885-96.
2. P. M. Som and H. D. Curtin, *Head and neck imaging,* Elsevier Health Sciences, 2011.
3. J. G. Batsaki, Williams & Willkins, 1979, 1120.
4. H. C. Thoeny, *Cancer Imaging*, 2007, **7(1)**, 52-62.
5. H. Abramczyk and B. Brozek-Pluska, *Chem. Rev.*, 2013, **113**, 5766-5781.
6. H. Abramczyk, B. Brozek-Pluska, E. Freysz and M. Tondusson, *J. Phys. Chem. C*, 2013, **117**, 4999-5013.
7. B. Brozek-Pluska, J. Musial, R. Kordek, E. Bailo, T. Dieing and H. Abramczyk, *Analyst*, 2012, **137(16)**, 3773-3780.
8. H. Abramczyk, B. Brozek-Pluska, J. Surmacki, J. Jablonska-Gajewicz and R. Kordek, *PBMB*, 2012, **108**, 74-81.
9. B. Brozek-Pluska, A. Jarota, J. Jablonska-Gajewicz, R. Kordek, W. Czajkowski and H. Abramczyk, *TCRT*, 2012, **4**, 317-331.
10. B. Brozek-Pluska, J. Jablonska-Gajewicz, R. Kordek and H. Abramczyk, *J. Med. Chem.* 2011, **54**, 3386-3392.
11. H. Abramczyk, B. Brozek-Pluska, J. Surmacki, J. Jablonska-Gajewicz and R. Kordek, *JBPC*, 2011, **2**, 158-169.
12. H. Abramczyk, B. Brozek-Pluska,J. Surmacki, J. Jablonska and R. Kordek, *J. Mol. Liq.*, 2011, **164**, 123-131.
13. H. Abramczyk, J. Surmacki, B. Brożek – Pluska, Z. Morawiec and M. Tazbir, *J. Mol. Struc.*, 2009, **924-926**, 175-182.
14. H. Abramczyk, I. Placek, B. Brożek – Płuska, K. Kurczewski, Z. Morawiec and M. Tazbir, *Spectroscopy an International Journal*, 2008, **22**, 113-121.
15. B. Brożek – Płuska, I. Placek, K. Kurczewski, Z. Morawiec, M. Tazbir and H. Abramczyk, *J. Mol. Liq*., 2008, **141**, 145-148.
16. H. Abramczyk, I. Placek, B. Brożek – Płuska, K. Kurczewski, Z. Morawiec and M. Tazbir, *ISRAPS Bulletin*, 2008, **20**, 16-20.
17. N. Stone and P. Matousek, *Cancer Res.*, 2008, **68(11)**, 4424-30.
18. N. Stone, C. Kendall, J. Smith, P. Crow and H. Barr, *Faraday Discuss*., 2004, **126**, 141-183.
19. A. J. Berger, T. W. Koo, I. Itzkan, G. Horowitz and M. S. Feld, *Appl. Opt.*, 1999, **38**, 2916-2926.
20. K. Virkler, I. K. Lednev, Anal. Bioanal. Chem., 2010, 396, 525-534.
21. T. R. Hata, T. A. Scholz, I. V. Ermakov, R. W. McClane, F. Khachik, W. Gellermann and L. K. Pershing, *J. Invest. Dermatol.,* 2000, **115**, 441-448.
22. C. D. Sudworth, J. K. Archer and D. Mann, *Optical Spectroscopy in Biomedicine III*, A. Mycek, ed., Vol. 5862 of Proc. SPIE (Optical Society of America, 2005), TuC3.
23. R. J. Swain and M. M. Stevens, *Biochem. Soc. Trans*., 2007, **35**, 544-549.
24. M. Hedegaard, Ch. Krafft, H. J. Ditzel, L. E. Johansen, S. Hassing and J. Popp, *Anal. Chem.*, 2010, **82**, 2797-2802.
25. K. E. Shafer-Peltier, A. S. Haka, J. T. Motz, M. Fitzmaurice, R. R. Dasari and M. S. Feld, *J. Cell. Biochem*., 2002, **87**, 125-137.
26. E. Bailo and V. Deckert, *Angew. Chem., Int. Ed.*, 2008, **47**, 1658-61.
27. J. Surmacki, J. Musiał, R. Kordek and H. Abramczyk, *Mol. Cancer*, 2013, **12**, 48.
28. T. Dieing, O. Hollricher and J. Toporski, *Confocal Raman Spectroscopy*, Springer - Verlag, Berlin Heidelberg, 2010.
29. F. S. Parker, *Applications of Raman and Resonace Raman Spectroscopy in Biochemistry.* Plenum Press, New York 1983.
30. J. Drenth, *Principles of Protein X-Ray Crystallography 2nd ed. Springer-Verlag, New York*, 1999.
31. R. K. Murray, D. K. Granner and V. W. Rodwell, *Harpers Illustrated Biochemistry*, The Mc Graw-Hill Companies, Inc. New York, 2006.
32. J. L. Lippert, D. Tyminski and P. J. Desmeules, *J. Am. Chem. Soc.* 1976, **101**, 5111-5121.
33. R. W. Williams and K. Dunker, *J. Mol. Biol.* 1981, **166**, 581-603.
34. M. Berjot, J. Marx and A. J. P. Alix, *J. Raman. Spectroscopy*, 1987, **18**, 289-300.
35. A. Rygula, K. Majzner, K. M. Marzec, A. Kaczor, M. Pilarczyk and M. Baranska, *J. Raman. Spectroscopy*, 2013, **44**, 1061-1076.
36. A. Barth, *Biochim. Biophys. Acta*, 2007, **1767**, 1073-1101.
37. S. B. Prusiner, *Science*, 1991, **252**, 1515-1522.
38. M. R. Goldsworthy and A. M. Vallence, *J. Neurosci.*, 2013, **33(32)**, 12910-12911.

Analyst Accepted Manuscript

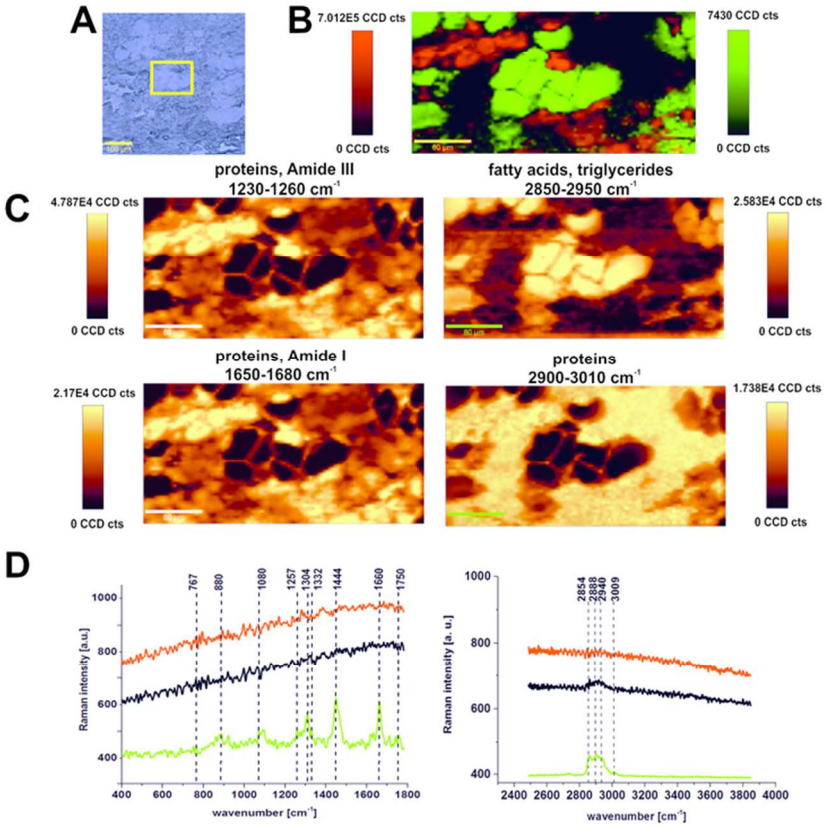

Fig. 1 Microscopy, Raman images and Raman spectra of the noncancerous salivary tissue of the patient P13. (A) Microscopy image (500x500 µm) composed of several single video images of the noncancerous salivary tissue, (B) Raman image (400x200 µm, resolution 1 µm) of the cryosectioned salivary tissue from the region marked in (A) obtained by the basis analysis, (C) images for the filters for spectral regions: 1230-1260 cm-1, 1650-1680 cm-1, 2850-2950 cm-1, 2900-3010 cm-1 (D) Raman spectra of the noncancerous salivary tissue. The colours of the Raman spectra in (D) correspond to the colours in the Raman image (B). Mixed areas are displayed as mixed colours. Integration time: 0.3 sec.
75x68mm (300 x 300 DPI)

Analyst Accepted Manuscript

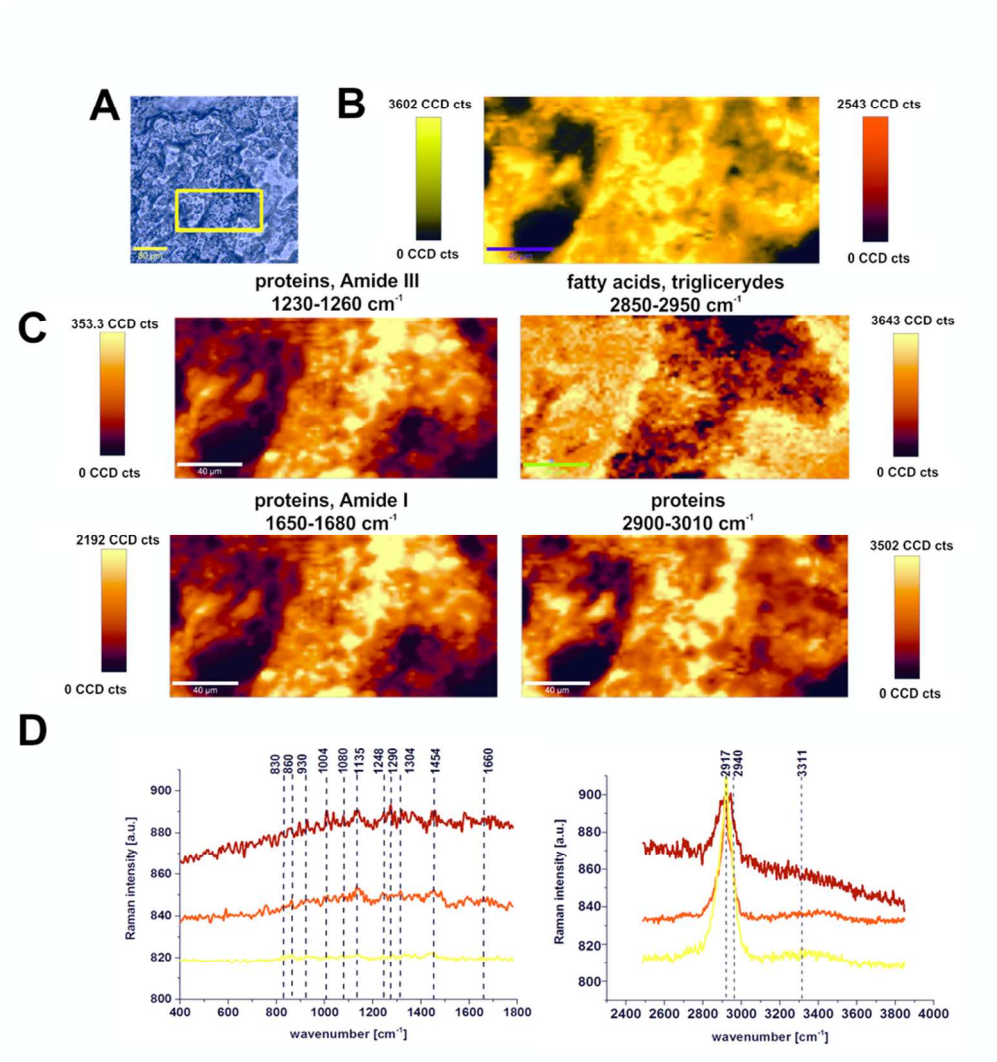

Microscopy, Raman images and Raman spectra of the cancerous salivary tissue of the patient P13. (A) Microscopy image (500x500 µm) composed of several single video images of the cancerous salivary tissue, (B) Raman image (350x350 µm, resolution 1 µm) of the cryosectioned salivary tissue from the region marked in (A) obtained by the basis analysis, (C) images for the filters for spectral regions: 1230-1260 cm-1, 1650-1680 cm-1, 2850-2950 cm-1, 2900-3010 cm-1 (D) Raman spectra of the cancerous salivary tissue. The colours of the Raman spectra in (D) correspond to the colours in the Raman image (B). Mixed areas are displayed as mixed colours. Integration time: 0.3 sec.
87x93mm (300 x 300 DPI)

Analyst Accepted Manuscript

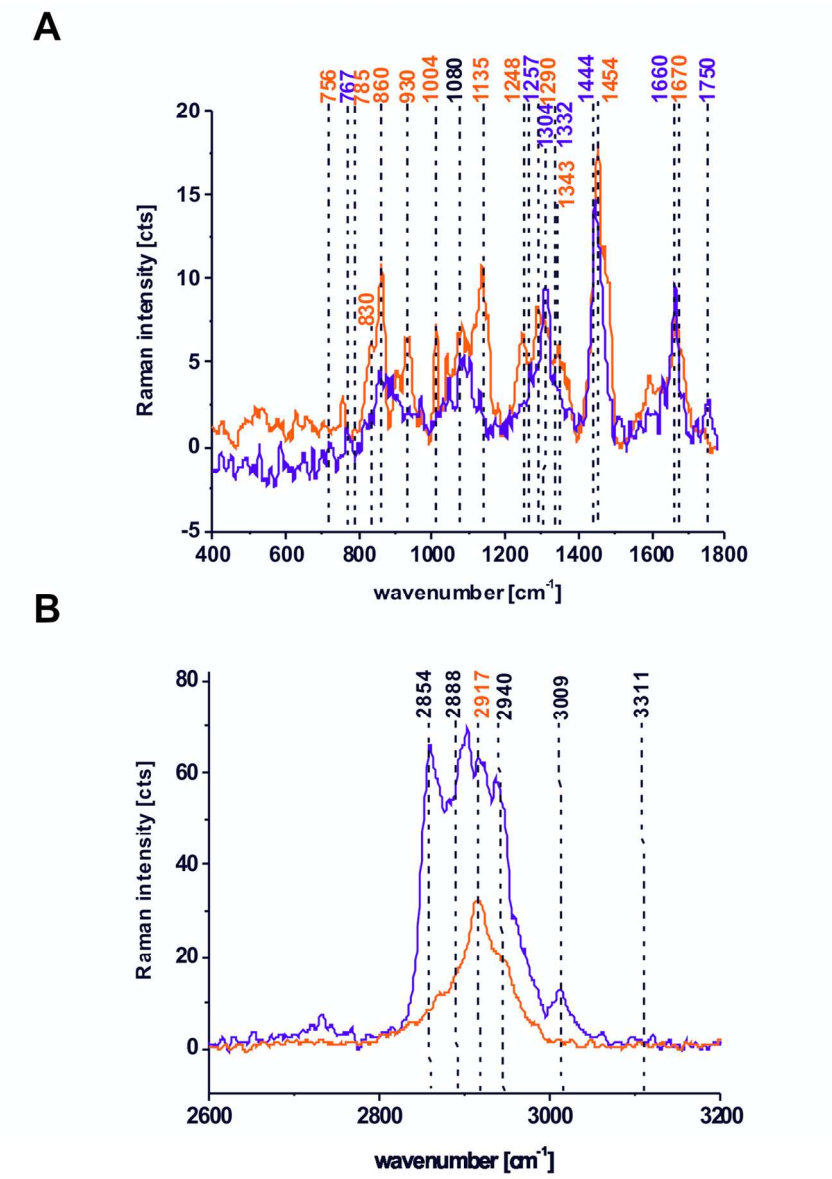

Fig. 3 Comparison of the mean Raman spectra of the noncancerous and the cancerous salivary tissues of the same patient P13, into spectroscopic regions (A) 400-1800 cm-1 and (B) 2600-3200 cm-1.
116x165mm (300 x 300 DPI)

Analyst Accepted Manuscript

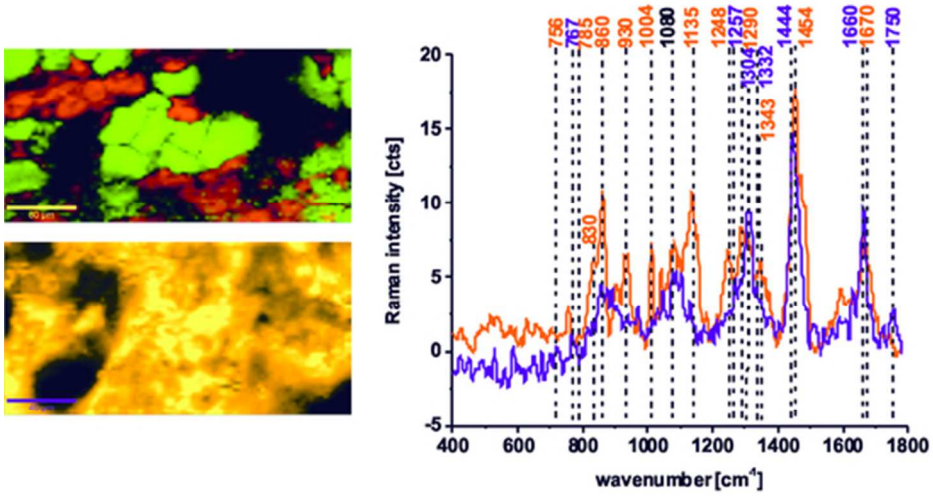

graphical abstract
49x25mm (300 x 300 DPI)

Analyst Accepted Manuscript